Supplementary Information for

Ultra-Narrow TaS_2 Nanoribbons

Jeffrey D. Cain[1,2,3†], Sehoon Oh[1,2†], Amin Azizi[1,3†], Scott Stonemeyer[1,2,3,4], Mehmet Dogan[1,2], Markus Thiel[1], Peter Ercius[5], Marvin L. Cohen[1,2], and Alex Zettl[1,2,3,*]

[1]*Department of Physics, University of California at Berkeley, Berkeley, CA 94720, USA*

[2]*Materials Sciences Division, Lawrence Berkeley National Laboratory, Berkeley, CA 94720, USA*

[3]*Kavli Energy NanoSciences Institute at the University of California at Berkeley and the Lawrence Berkeley National Laboratory, Berkeley, CA 94720, USA*

[4]*Department of Chemistry, University of California at Berkeley, Berkeley, CA 94720, USA*

[5]*The Molecular Foundry, Lawrence Berkeley National Laboratory, Berkeley, CA 94720 USA*

†These authors contributed equally

*e-mail: azettl@berkeley.edu

This PDF file includes:

Materials and Methods

Materials Synthesis*:* Multi-walled carbon nanotubes (CNTs) (Cheap tubes) were opened *via* oxidation at high temperature. They were heated to 515 ℃ for 1 hour in air, before the filling step. For filling with TaS_2 NRs, the opened CNTs, along with elemental sulfur and tantalum powders were sealed under high vacuum (10^{-6} Torr) in 2 mm diameter quartz ampules and held at 760 ℃ for 1 week, then to cooled room temperature naturally.

Materials Characterization: The filled CNTs are dispersed in isopropyl alcohol by bath sonication for 1 hour and drop-cast onto lacey carbon transmission electron microscope grids for imaging. Transmission electron microscope imaging was carried out at 80 keV on a JEOL 2010 microscope. Atomic-resolution STEM imaging is completed at the National Center for Electron Microscopy on TEAM 0.5 which is a Titan 80-300 with an ultra-twin pole piece gap, DCOR probe aberration corrector and was operated at 80 kV and semi-convergence angle of 30 mrad. Images were acquired using the ADF-STEM detector with an inner angle of 60 mrad and a beam current of approximately 70 pA. An aberration-corrected FEI Titan3 (60−300) equipped with a SuperX EDS system at 80 kV was also used for the imaging and spectroscopy. Elemental mapping was performed in the STEM mode at 80 kV with a 7 min acquisition time.

STEM simulations were done using Prismatic's prism algorithm with parameters that matched the experiments. In detail for each simulation, we used a 52.92 Å square simulation box, 80 kV accelerating voltage, 30 mrad convergence semi-angle, 0.04 Å/pixel sampling, 1 Å slice size, interpolation factor 4 and 50 frozen phonon calculations. After completion, the simulation data was convolved with a 1.3 Å source size to match the contrast seen in the experiment images. Noise was added following Poisson counting statistics to match the 70 pA experimental beam current. This allowed us to interpret the positions of atoms based on the

approximate Z-contrast in the images and to compare the projection images to the DFT simulated structures.

Computational Methods: We use the generalized gradient approximation[1], norm-conserving pseudopotentials[2], and localized pseudo-atomic orbitals for the wavefunction expansion as implemented in the SIESTA code[3]. The spin–orbit interaction is considered using fully relativistic j-dependent pseudopotentials[4] in the l-dependent fully-separable nonlocal form using additional Kleinman–Bylander-type projectors[5]. We use a 64×64×18 Monkhorst–Pack *k*-point mesh for 2H-bulk, a 64×64×1 mesh for 1H-ML, a 1×64×1 mesh for 1H-NR without boundaries, and a 1×9×1 mesh for 1H-NR with boundaries. Real-space mesh cut-off of 1000 Ry is used for all of our calculations. The van der Waals interaction is evaluated using the DFT-D2 correction[6]. Dipole corrections are included to reduce the fictitious interactions between layers generated by the periodic boundary condition in our supercell approach[7].

Encapsulation in CNT: To investigate the effects of encapsulation of the TaS_2 nanoribbons (NRs) inside the carbon nanotubes (CNTs), separately relaxed atomic positions of TaS_2-NRs isolated in vacuum and empty CNTs are used. Further relaxations are not performed. We then calculate the charge transfers between NRs and CNTs. The calculated charge transfer (q) from CNTs to 1H-TaS_2 NRs is 0.0192 e/Ta atom, where e is the electron charge. Note that q is much smaller than those for the transition metal tricalcogenides such as $NbSe_3$[8], $HfTe_3$[9], and Hf_2Te_9 molecular chain[10].

Magnetic Moments: We perform fully magnetic calculations with spin–orbit interaction. We start with various magnetic moments in the self-consistent calculation, but find no significant magnetic moment in any of the converged calculation results. After carefully checking the

magnetic moments, we perform self-consistent calculations again assuming the time-reversal symmetry.

Topological Properties: Because of the presence of the mirror symmetry in prismatically coordinated TaS_2 NRs combined with the time-reversal symmetry, the Zak phases of the bands are quantized[11]. For a TaS_2-NR with a finite total gap, which is not the case in this study but might be the case with smaller width, the topological invariance of the NR can be tuned by controlling the charge state using doping or gating as reported in recent studies[9,12].

References

(1) Perdew, J. P.; Burke, K.; Ernzerhof, M. Generalized Gradient Approximation Made Simple. *Phys. Rev. Lett.* **1996**, *77* (18), 3865–3868. https://doi.org/10.1103/PhysRevLett.77.3865.

(2) Troullier, N.; Martins, J. L. Efficient Pseudopotentials for Plane-Wave Calculations. *Phys. Rev. B* **1991**, *43* (3), 1993–2006. https://doi.org/10.1103/PhysRevB.43.1993.

(3) Soler, J. M.; Artacho, E.; Gale, J. D.; García, A.; Junquera, J.; Ordejón, P.; Sánchez-Portal, D. *The SIESTA Method for Ab Initio Order-N Materials Simulation*; 2002; Vol. 14.

(4) Bachelet, G. B.; Schlüter, M. Relativistic Norm-Conserving Pseudopotentials. *Phys. Rev. B* **1982**, *25* (4), 2103–2108. https://doi.org/10.1103/PhysRevB.25.2103.

(5) Theurich, G.; Hill, N. A. Self-Consistent Treatment of Spin-Orbit Coupling in Solids Using Relativistic Fully Separable Ab Initio Pseudopotentials. *Phys. Rev. B - Condens. Matter Mater. Phys.* **2001**, *64* (7), 073106. https://doi.org/10.1103/PhysRevB.64.073106.

(6) Grimme, S. Semiempirical GGA-Type Density Functional Constructed with a Long-Range Dispersion Correction. *J. Comput. Chem.* **2006**, *27* (15), 1787–1799. https://doi.org/10.1002/jcc.20495.

(7) Cohen, M. L.; Schlüter, M.; Chelikowsky, J. R.; Louie, S. G. Self-Consistent Pseudopotential Method for Localized Configurations: Molecules. *Phys. Rev. B* **1975**, *12* (12), 5575–5579. https://doi.org/10.1103/PhysRevB.12.5575.

(8) Pham, T.; Oh, S.; Stetz, P.; Onishi, S.; Kisielowski, C.; Cohen, M. L.; Zettl, A. Torsional Instability in the Single-Chain Limit of a Transition Metal Trichalcogenide. *Science* **2018**, *361* (6399), 263–266. https://doi.org/10.1126/science.aat4749.

(9) Meyer, S.; Pham, T.; Oh, S.; Ercius, P.; Kisielowski, C.; Cohen, M. L.; Zettl, A. *Metal-Insulator Transition in Quasi-One-Dimensional HfTe3 in the Few-Chain Limit*.

(10) Pham, T.; Oh, S.; Stonemeyer, S.; Shevitski, B.; Cain, J. D.; Song, C.; Ercius, P.; Cohen, M. L.; Zettl, A. Emergence of Topologically Nontrivial Spin-Polarized States in a Segmented Linear Chain. *Phys. Rev. Lett.* **2020**, *124* (20), 206403. https://doi.org/10.1103/PhysRevLett.124.206403.

(11) Zak, J. Berrys Phase for Energy Bands in Solids. *Phys. Rev. Lett.* **1989**, *62* (23), 2747–2750. https://doi.org/10.1103/PhysRevLett.62.2747.

(12) Cao, T.; Zhao, F.; Louie, S. G. Topological Phases in Graphene Nanoribbons: Junction

States, Spin Centers, and Quantum Spin Chains. *Phys. Rev. Lett.* **2017**, *119* (7), 076401. https://doi.org/10.1103/PhysRevLett.119.076401.

Figures:

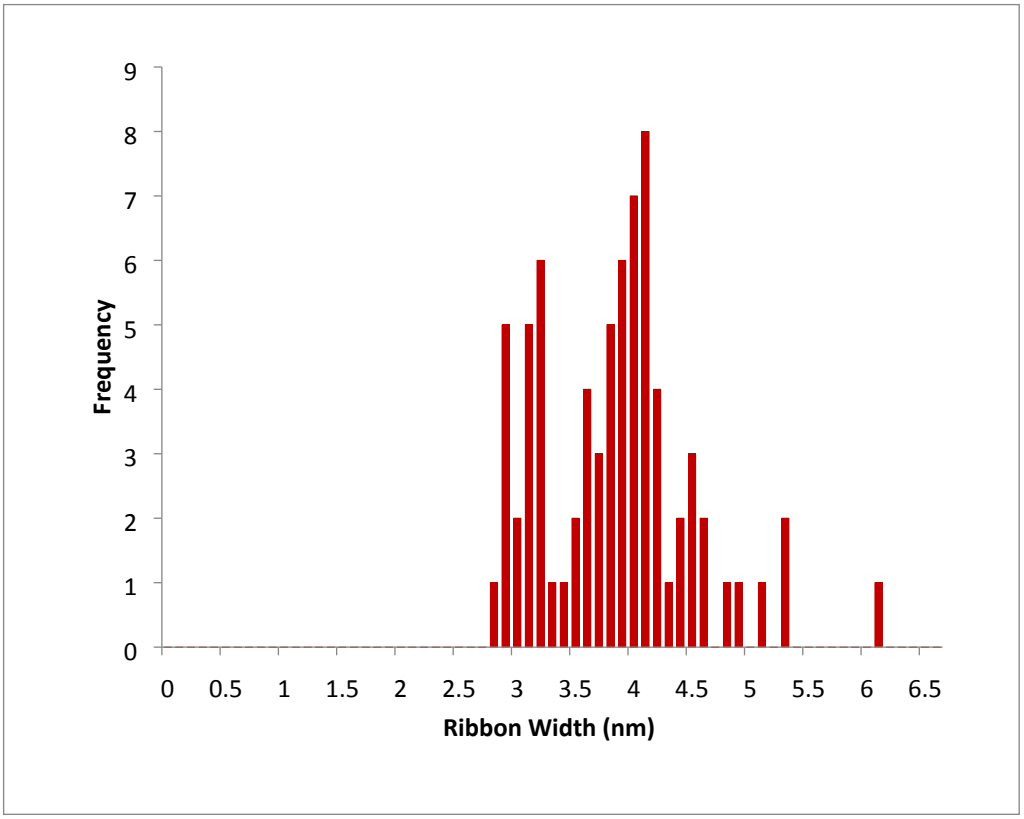

Fig. S1. Histogram of TaS_2 nanoribbon widths.

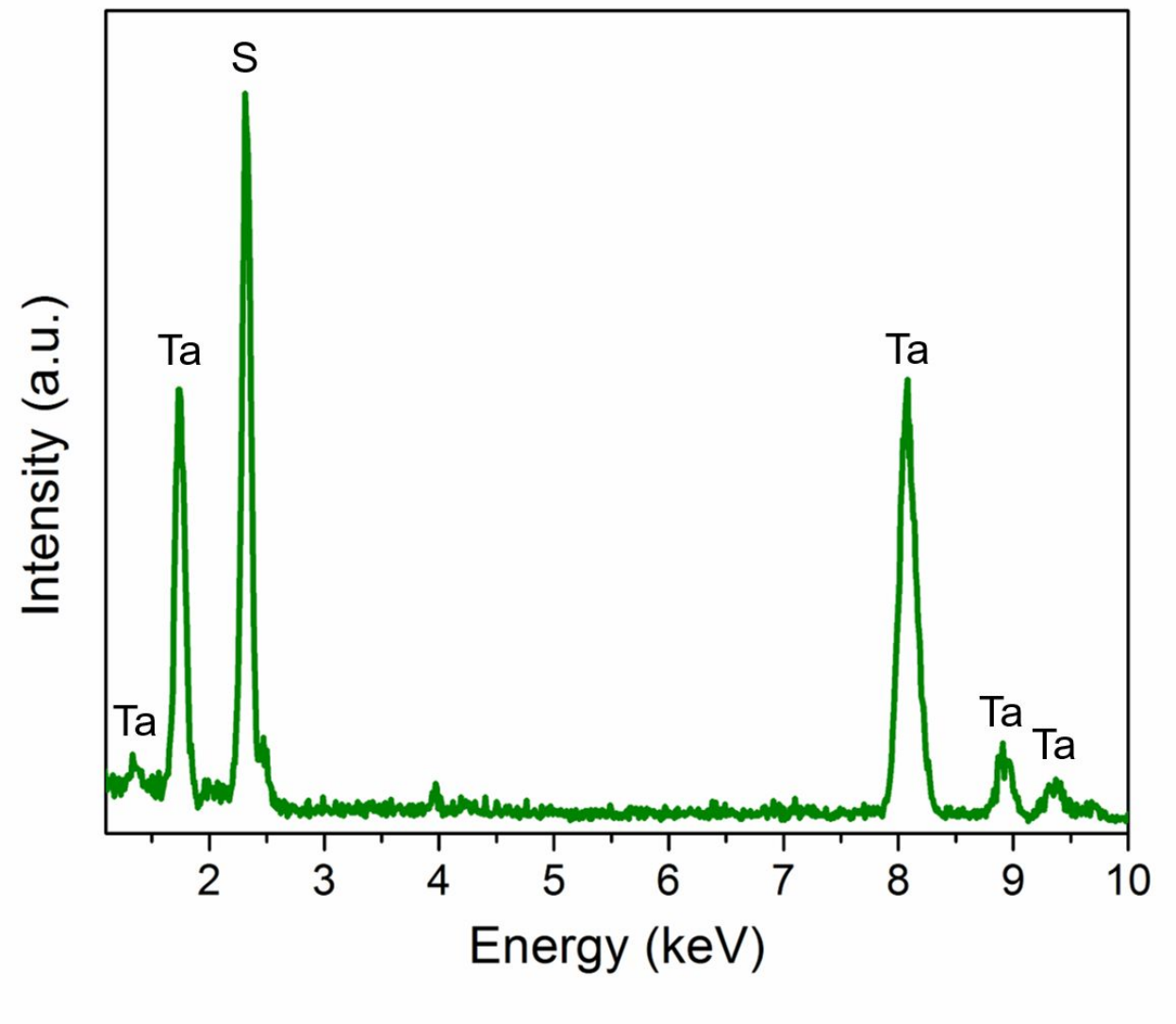

Fig. S2. Energy dispersive x-ray spectroscopy (EDS). EDS Spectrum.

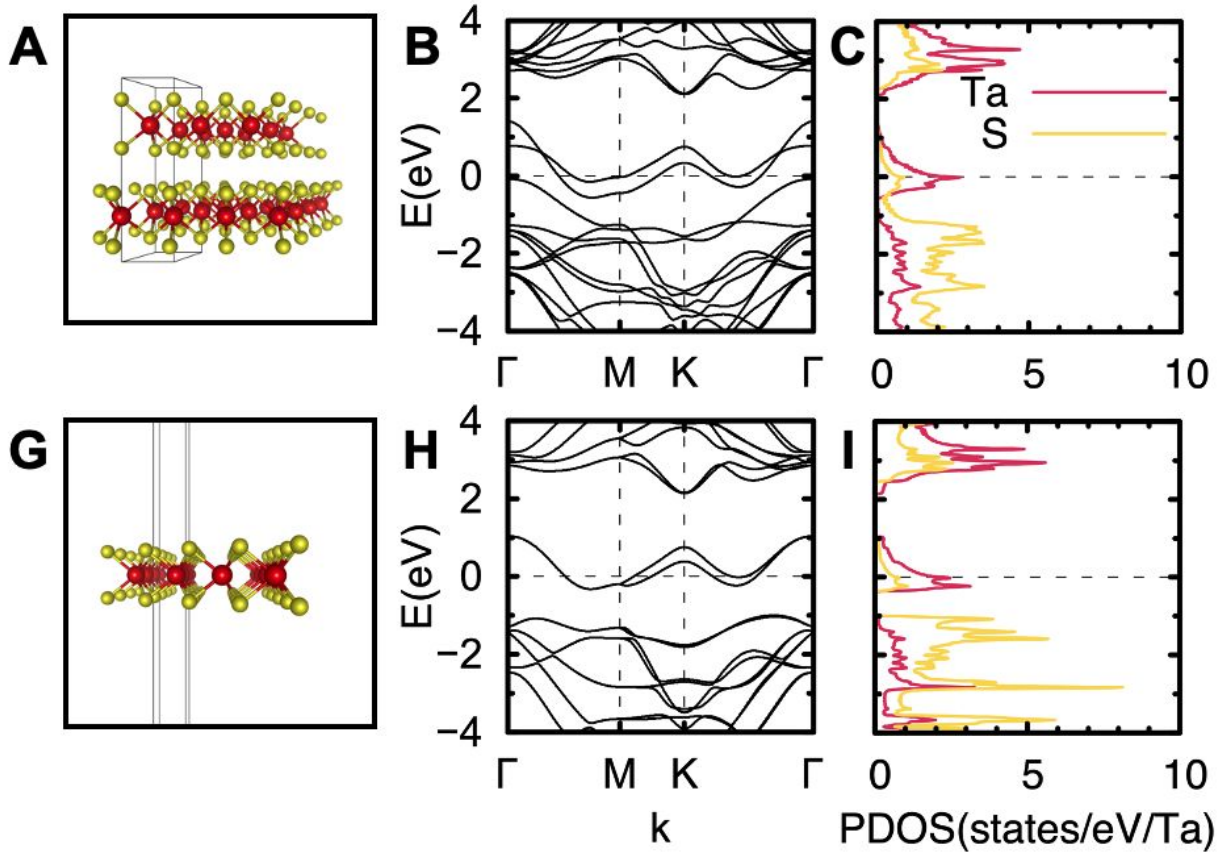

Fig. S3. Atomic and electronic structures of the TaS_2 bulk and monolayer (ML). The atomic and electronic structures of TaS_2 with prismatic coordination of **(A-C)** 2H-bulk, and **(D-F)** 1H-ML are shown. In the 1st column, the atomic structures obtained from density functional theory (DFT) calculations are shown where Ta and S atoms are represented by red and yellow spheres, respectively, and the unit-cell is represented by black frames. In the 2nd column, the electronic band structures are shown where the Fermi energy is set to zero. In the 3rd column, the projected density of states (PDOS) are shown, where the density of states projected to Ta and S atoms are represented by red and yellow lines, respectively.

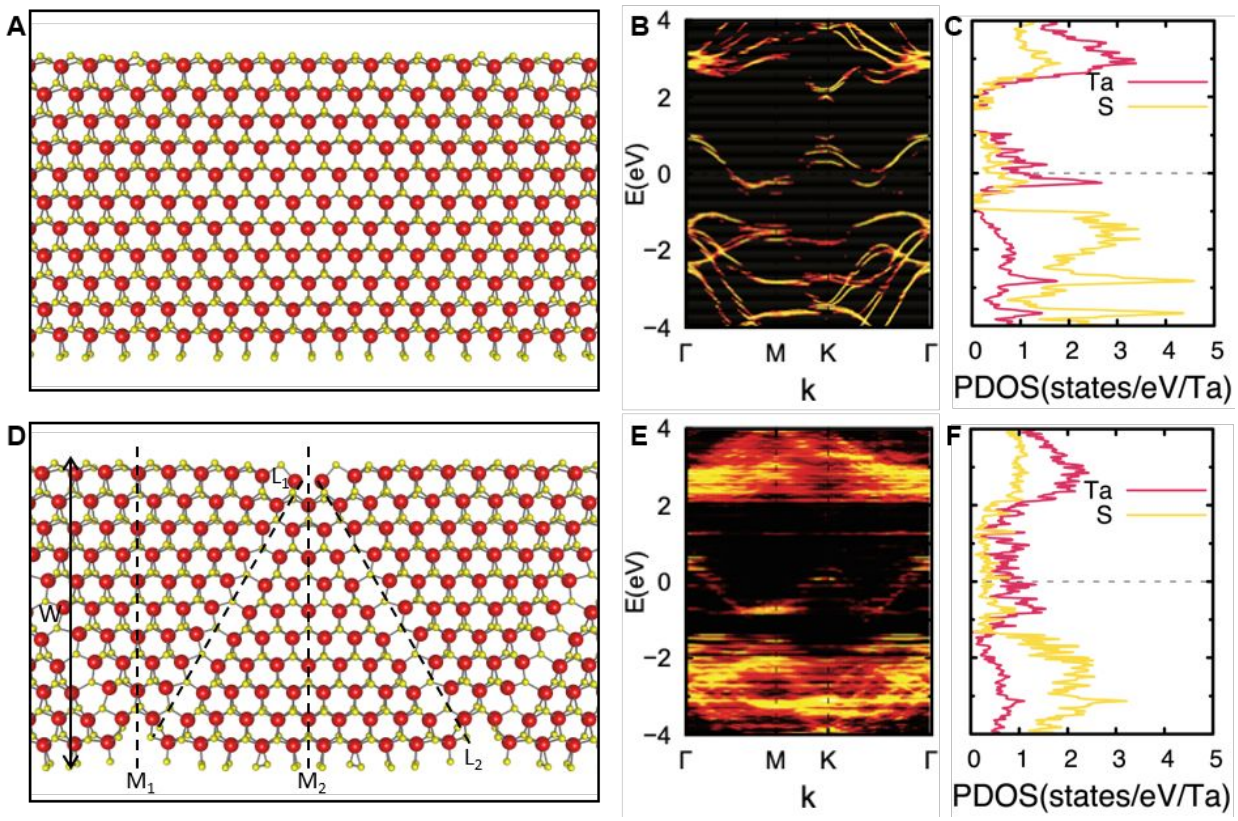

Fig. S4. Atomic and electronic structure of TaS_2 NRs with and without defect arrays. (A-C) The atomic and electronic structures of the NR of W=3.29 nm without the zigzag defect are shown. **(A)** The atomic structure in planar view, **(B)** the electronic band structure and **(C)** the PDOS of the NR are shown. **(D-H)** The atomic and electronic structures of NR of W=3.34 nm with zigzag defect array are shown. **(D)** The atomic structure of the NR is shown in the planar view, where the zigzag boundaries of S vacancies are represented by the dashed lines denoted as L_1 and L_2, and the mirror planes are represented by vertical dashed lines denoted as M_1 and M_2. **(E)** The electronic band structure and **(F)** the PDOS of the NR are shown. In the atomic structures, Ta and S atoms are represented by red and yellow spheres, respectively. The bands in **(B)** and **(E)** are unfolded with respect to the unit-cell of the primitive ML. The density of states projected to Ta and S atoms are represented by red and yellow lines, respectively. The Fermi energy is set to zero.